DOI 10.1007/s11182-019-01664-5

Russian Physics Journal, Vol. 61, No. 12, April, 2019 (Russian Original No. 12, December, 2018)

PECULIARITIES OF STRUCTURE AND PHASE COMPOSITION OF TERNARY NiMn–NiTi ALLOYS WITH A QUASI-BINARY CROSS-SECTION

E. S. Belosludtseva,[1] E. B. Marchenkova,[1] A. V. Pushin,[1,2] V. G. Pushin,[1,2] and A. É. Svirid[1]

UDC 538.911

The influence of a chemical composition on the phase composition, stability, and crystal structure type of the austenitic and martensitic ternary NiMn–NiTi *alloys with a quasi-binary cross-section is analyzed. The temperature-concentration limits of their existence are determined. It is found out that doping of these alloys with titanium decreases the critical temperatures of thermoelastic martensitic transformations compared to those of the basic binary intermetallic compound* NiMn*. In the alloys, doped with more than 15 at.% titanium, phase decomposition is observed, followed by the formation of titanium-rich* (Ni_3Ti) *ternary precipitates of the 4H-HCP type, which form a Widmanstatten substructure.*

Keywords: phase composition, microstructure, decomposition, stratification, martensite.

INTRODUCTION

An investigation of structural, multi-functional shape-memory alloys, undergoing different thermoelastic martensitic transformations (TMTs) under the action of temperature, deformation, or magnetic field, is of scientific and practical importance [1–3]. The fine structure and physical properties of binary titanium-doped alloys of the Ni–Mn system have been studied in a large number of works [4–8], and a conclusion was drawn on a thermo-elastic mechanism of the $B2 \rightarrow L1_0$ and $B2 \rightarrow$ 10M martensitic transitions; in [7] the TMT diagrams were constructed and their critical temperatures were determined. In a number of Russian and foreign publications it was reported that ternary $Ni_{50}Mn_{50-x}Ti_x$ alloys with a quasi-binary cross-section in addition to the martensitic transformation undergo antiferrromagnetic ordering [8]. There have been practically no detailed microstructural investigations of these alloys. Nevertheless, it could be concluded from the literature data that the solubility of Mn in Ni is higher than that in Ti [9]. The studies dealing with the construction of phase diagrams and investigation of phase compositions of NiMn-based ternary alloys are not numerous [7–9]. Despite this fact, an attempt was made to generalize the data accumulated on the Ni–Mn–Ti system [10]. An example of a ternary-diagram cross-section is given in Fig. 1, wherein crossed circles indicate the compositions close to those selected for the present study.

The microstructure and chemical compositions of the metallographic sections were characterized using a Quanta-200 Pegasus scanning electron microscope (SEM), and an electron-microscopy examination of thin foils was performed in the JEM 200CX, CM 30 and Tecnai G^2 Twin transmission electron microscopes (TEM) of the Collaborative Access Center "Testing Center of Nanotechnology and Advanced Materials" at the Institute of Metal Physics of the Ural Branch of the RAS. The phases were identified by the method of microdiffraction from a selected

[1]M. N. Mikheev Institute of Metal Physics of the Ural Branch of the Russian Academy of Sciences, Ekaterinburg, Russia, e-mail: ebelosludceva@mail.ru; em1104@mail.ru; avpushin@rambler.ru; pushin@imp.uran.ru; svirid2491@rambler.ru; [2]Ural Federal University named after the first President of Russia B. N. Yeltsin, Ekaterinburg, Russia. Translated from Izvestiya Vysshikh Uchebnykh Zavedenii, Fizika, No. 12, pp. 103–108, December, 2018. Original article submitted October 5, 2018.

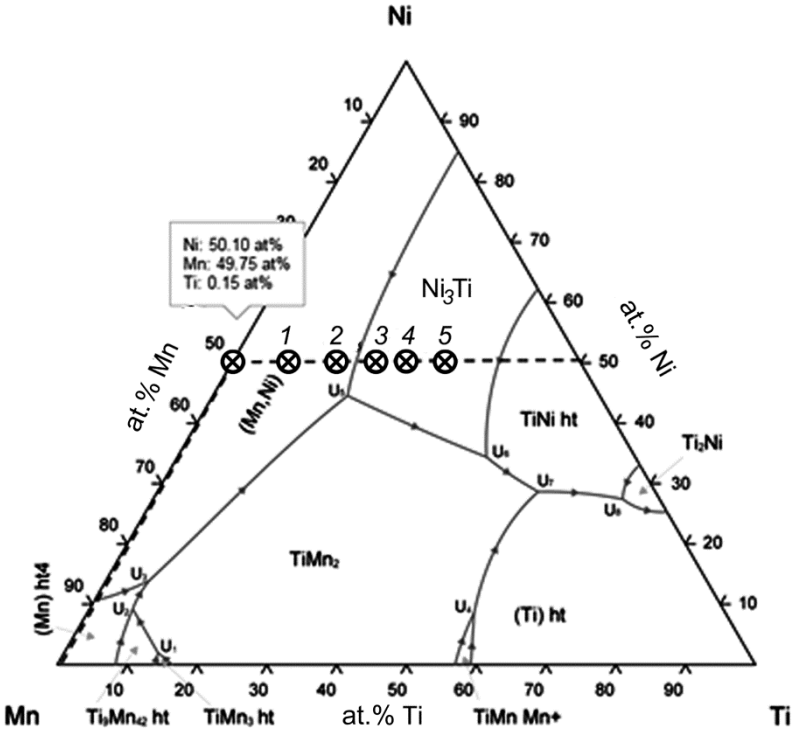

Fig. 1. Ternary phase diagram of the Ni–Mn–Ti system in a liquidus projection [10], crossed circles (numbered *1* through *5*) in the diagram indicate the alloy compositions in at.%: 50.05 Ni, 41.95 Mn, 8.00 Ti (*1*), 50.00 Ni, 35.07 Mn, 14.93 Ti (*2*), 50.17 Ni, 29.35 Mn, 20.48 Ti (*3*), 50.15 Ni, 25.00 Mn, 24.85 Ti (*4*), 50.11 Ni, 19.56 Mn, 30.33 Ti (*5*).

area. A phase analysis by X-ray diffraction (XRD) was performed in a DRON-3M diffractometer in the monochromatized CuK_α emission.

In the present study, a systematic investigation of the influence of doping with titanium on the features of microstructure, phase composition, and phase transformations is performed in quasi-binary $Ni_{50}Mn_{50-x}Ti_x$ alloys.

The purpose of this work is to investigate the phase and structural transformations in the alloys of the $Ni_{50}Mn_{50-x}Ti_x$ system and to determine the dependence of their phase composition on the concentration of the doping chemical elements.

1. MATERIAL AND EXPERIMENTAL PROCEDURE

For investigations we selected a number of ternary quasi-binary alloys $Ni_{50}Mn_{50-x}Ti_x$ (x = 5, 10, 15, 20, 25, 30 at.%), which were synthesized relying on the principle of substitution of titanium for magnesium. The chemical compositions of the alloys after their melting were determined in order to select the samples for further investigations. An admissible deviation from the stoichiometric composition was no more than ±0.2 at.%.

The model alloys of precise compositions were melted from high-purity components: electrolytic nickel and magnesium (purity 99.99%), as well as titanium iodide (99.8%) by the method of electric-arc welding in a purified argon atmosphere. For the sake of homogenization, the alloys were subjected to multiple remelting (no less than three times), followed by prolonged annealing in vacuum at the temperature (1123 ± 25) K. The ingots were sliced into plates in an electric spark machine and subsequently annealed in the β-state of (*B*2)-phase at the temperature 1123 K for 30 h, followed by quenching into water. The plate surfaces were mechanically ground and electrochemically etched in order

TABLE 1. Phase Compositions and Crystal Lattice Types of the $Ni_{50}Mn_{50-x}Ti_x$ Alloy System from the Room-Temperature XRD Data

x, at.%	Phase structure type	Crystal lattice parameters, nm		
		a	b	c
0	$L1_0$ (2M)	0.3740		0.3520
5	$L1_0$ (2M)	0.3746		0.3498
	10M	0.4400	0.2699	2.1109
10	10M	0.4450	0.2728	2.1150
15	$B2$	0.2976		
20	$B2$	2.985		
	$L2_1$	5.970		
	Ni_3Ti – HCP (4H)	0.517		0.835

to remove the hardened layer, followed by electropolishing in a solution of acetic and perchloric acids (80% – CH_3COOH, 20% – $HClO_4$) at the temperature 2–5°C and the voltage 12–15 V for 10–20 s, depending on the specimen area. The cathode was manufactured from titanium foil.

2. EXPERIMENTAL RESULTS AND DISCUSSION

Phase analysis by X-ray diffraction (XRD). Using the XRD data, phase compositions of all alloys investigated at room temperature have been determined. It was found out that depending on doping the crystal lattice type of the martensite changed. For instance, the $Ni_{50}Mn_{50}$ and $Ni_{50}Mn_{40}Ti_{10}$ alloys at room temperature were in the martensitic state, but the martensite had a tetragonal or more complex multilayer lattice [7]. The crystal lattice type was determined during interpretation of the X-ray spectra; the lattice type of the $Ni_{50}Mn_{50}$ alloy corresponded to a tetragonal $L1_0$ (2M)-lattice, while the alloy with 5 at.% Ti, found in the boundary region, was characterized by a dual-phase structure: single- (2M) and five-layer (10M) modulated structures [7]. In the alloy with 10 at.% Ti, the martensitic phase had a 10M structure type. The parameters of these phases are listed in Table 1.

The XRD analysis has also revealed that the $Ni_{50}Mn_{35}Ti_{15}$ alloy at room temperature was in a state of the $B2$-austenite with the lattice parameter a = 0.2976 nm [7] (Table 1). A TMT in this alloy occurs at the temperature lower than room temperature and is also accompanied by the formation of a 10M phase. Table 1 presents the types of all phases and crystal lattice parameters of the alloys with the content of titanium from 0 to 20 at.%. Using the XRD data, it has been determined that the alloys containing from 15 to 30 at.% Ti have a tendency towards phase separation (Fig. 2). From the X-ray data it has been also found out that the precipitated phase has a close-packed hexagonal crystal lattice of the Ni_3Ti type with the c/a ratio close to 1.615. Its parameters are also given in Table 1. It is notable that in the alloys doped with 20 at.% Ti, along with the $B2$ superstructure, a higher-rank superstructure – $L2_1$, has been revealed, whose availability in the alloy is validated by the characteristic reflections in the X-ray pattern (Fig. 2).

Microstructure of the $Ni_{50}Mn_{50-x}Ti_{50}$ alloys. TEM- and SEM investigations were performed at room temperature using the same cast specimens which were investigated by the XRD-method. Figure 3 presents TEM-images of the structures of the cast alloys $Ni_{50}Mn_{50}$, $Ni_{50}Mn_{40}Ti_{10}$, and $Ni_{50}Mn_{30}Ti_{20}$.

It is evident that the twinned structure of the binary alloy martensite is characterized by the packet-platy structure (Fig. 3*a*). In finer grains (as small as 5 μm) only one packet was generally present. In coarser grains, the adjacent packets joined each other along the inter-packet boundaries, which in the general case were not planar, though they separated the coherently joined packets of twin-oriented tetragonal plates. The microstructure of the alloy doped with 10 at.% Ti is characterized by a more complex morphology (Fig. 3*b*). The packet morphology of the martensitic plates is not homogeneous: an opposite wedging-out of the needle of martensite crystals was observed, whose packets joined inside the grain. Also, there were internal twins finer than those in a binary alloy. The elastic stresses in the foil are observed to form extinction contours in the image. Moreover, there are equidistant extra reflections in the electron

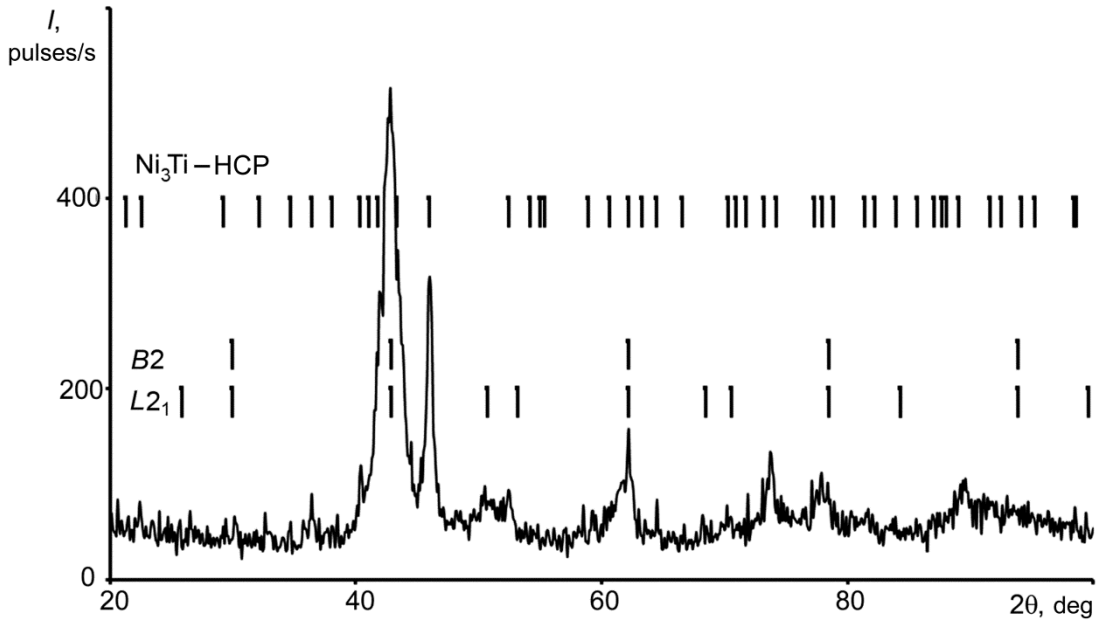

Fig. 2. XRD spectrum of the $Ni_{50}Mn_{30}Ti_{20}$ alloy and its interpretation in the form of line-diagrams of the phases $B2$, $L2_1$ and HCP-4H (of the Ni_3Ti type).

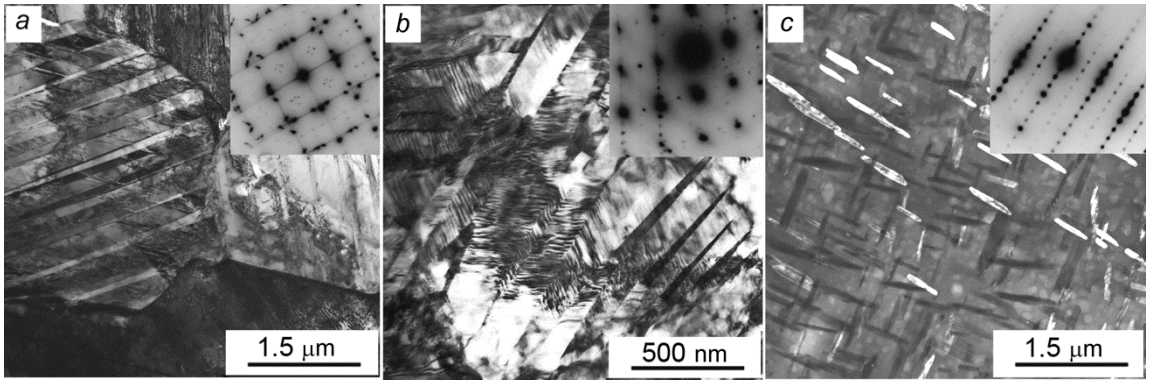

Fig. 3. TEM-images of the structure of experimental alloys (*a* – $Ni_{50}Mn_{50}$, *b* – $Ni_{50}Mn_{40}Ti_{10}$, *c* – $Ni_{50}Mn_{30}Ti_{20}$) and the respective electron diffraction patterns (in inserts).

diffraction pattern, which are nearly multiple of the 1/5 <110> reciprocal *B*2-lattice, from the five-layer orthorhombic lattice 10M (Fig. 3*b*).

TEM-investigations of the alloys, starting from the nominal composition $Ni_{50}Mn_{35}Ti_{15}$, in addition to *B*2-austenite revealed another phase with the 4H-HCP-type structure, as was the case with the XRD-analysis. In the alloy with 15 at.% Ti, it is presented by separate isolated plates. In the *B*2- alloys doped with 20–30 at.% Ti, the precipitates of the second-phase plates are located in the image at the angles 60, 90 and 120° (Fig. 3*c*). It is evident that in the cast alloys with 15– 30 at.% Ti there are diffusion-induced phase transformations not suppressed by quenching.

SEM-images of the microstructure of the $Ni_{50}Mn_{30}Ti_{20}$ and $Ni_{50}Mn_{20}Ti_{30}$ alloys are presented in Fig. 4. According to the microanalysis, their chemical composition in the regions of excessive phases differs from the nominal composition by an excessive content of Ni within 3–9 at.% and smaller contents of Mn and Ti.

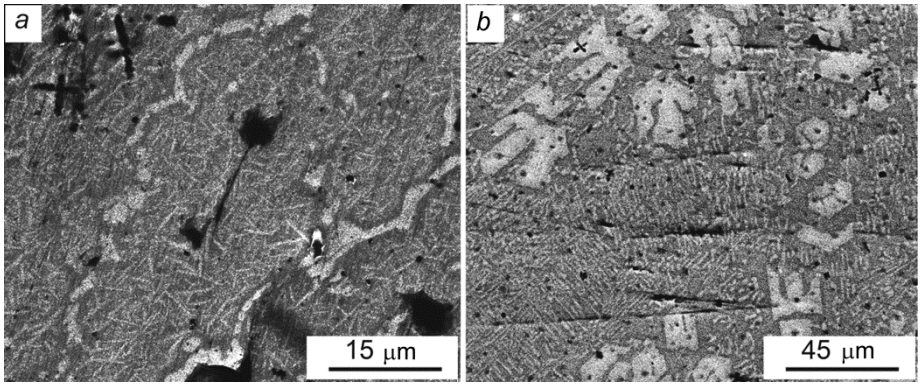

Fig. 4. Secondary-electron SEM-images of the alloy structure: *a* – $Ni_{50}Mn_{30}Ti_{20}$, *b* – $Ni_{50}Mn_{20}Ti_{30}$.

It is evident that the contrast from the second-phase precipitates is present not only along the grain boundaries but also in their bulk, forming Widmanstatten-type morphology. The precipitates are uniformly distributed over the plane of the metallographic section in the form of characteristic "needles", the majority of which are located with respect to each other at certain angles close to 60 and 90°. A trace analysis allowed determining the planes and directions of the occurrence of second-phase precipitates, specifically $\{011\}<01\bar{1}>_{B2}$. As it is well known, the angle between the normals to the family of planes of the {110} type is found to be 90 and 120°, and between the planes exactly 60 and 90°.

The interpretation of the X-ray and electron diffraction patterns (Fig.3 *c*) suggests that the observed phase precipitates formed in the *B*2-austenite matrix possess a complex four-layer hexagonal crystal lattice of the 4H-type. Higher-power TEM- and especially SEM-images of the alloys allow distinguishing a microstructure similar to dendritic or eutectoid structure. Metallographic sections of the $Ni_{50}Mn_{30}Ti_{20}$, $Ni_{50}Mn_{25}Ti_{25}$ and $Ni_{50}Mn_{20}Ti_{30}$ alloys also reveal complex distribution patterns of both phase and chemical compositions. Furthermore, the second-phase precipitates of different dispersion levels are quite uniformly distributed over the metallographic section planes (Fig. 4). Their local elemental composition, according to the chemical microanalysis data, differs by an excessive content of Ni (by 3–9 at.%) and, respectively, a smaller content of Mn and Ti compared to the nominal composition of the *B*2-matrix. The data of TEM examination of the alloy foils demonstrate that there are colonies of plate-like particles arranged in the Widmanstatten-type manner with the habitus planes $(001)_{HCP} \parallel \{110\}_{B2}$.

The electron diffraction patterns of the *B*2-alloys, doped with 15 to 30 at.% Ti, contain diffusion scattering strands (DSSs) along <110>* in different reciprocal lattice sections of the *B*2-austenite in the form of extended and shortened lines and extra reflections in the vicinity of Bragg reflections. The extra reflections are accounted for by the DSSs 'piercing' the Ewald sphere along the <110>* directions not lying in the planes of the electron diffraction patterns. They are caused by the short-range atomic displacement order (SDO) in the metastable *B*2-austenite matrix of the alloys [1–3], which in the electron-microscopy images is characterized by the deformation-induced tweed contrast.

An analysis of the well-known literature data implies that the diffusion effects along the {111}* planes of the reciprocal lattice appear 100–150° earlier than the onset of the martensitic transformation [1, 2]. It is known that during cooling (approaching to M_s) the intensity and resolution of the strands of the <110>* and <112>* types and in the positions close to 1/3<110>*, 1/2<110>*, and 1/3<112>* are especially high. The intensity and regularity of the tweed contrast also increase. Flat layers of scattering along {111}* in the BCC-crystals are interpreted as a consequence of crystal destabilization with respect to the displacements of close-packed atomic chains along <111>, strands along <110>* and <112>* – towards planar displacements of atoms across $\{110\}<1\bar{1}0>$ and $\{112\}<11\bar{1}>$, which could be treated as a consequence of progressive correlated displacements of close-packed rows along <111> in the close-packed "soft-shear" planes [1–3].

Consequently, the increase in and evolution of the diffusion scattering of electrons (flat layers{111}* → strands <110>* and <112>* → satellites in weakly incommensurate positions) and tweed contrast observed in the *B*2-alloys $Ni_{50}Mn_{50-x}Ti_x$, which are metastable towards TMTs, are evidence of their 'distortion' origin, caused by the

decreased stability of the BCC-matrix of these alloys to atomic displacements. It is reasonable to treat the evolutionary increase of ordering in the shuffling (short-wave) atomic displacements along the soft-shear systems $\{110\}<1\bar{1}0>$ and $\{112\}<11\bar{1}>$ as a certain continuous intra-phase transition of the 2-nd kind from the localized short-range order of atomic displacements towards intermediate nanodomain shear structures. The short-range atomic displacement order corresponds to the stages of 'continuous strands' and intermediate shear structures – to the 'satellite' stage [1–3].

CONCLUSIONS

1. The types of crystal lattices of the martensitic phases $L1_0$ and 10M, formed in the $Ni_{50}Mn_{50-x}Ti_x$ alloys of a wide range of compositions (x = 0–15 at.%), have been identified and the parameters of their atomic-crystalline structure have been determined.

2. The ternary, quasi-binary $Ni_{50}Mn_{50-x}Ti_x$ alloys with the content of Ti more than 15 at.% undergo disintegration during crystallization followed by precipitation of the ternary, long-period ordered HCP – 4H phase of the Ni_3Ti type enriched in nickel by 3–9 at.% and hence depleted in magnesium and titanium compared to the $B2$-matrix of the alloys. These precipitates are distributed along the grain boundaries and also in the bulk of the grains forming Widmanstatten-type structures.

3. It has been found out that the austenite of these alloys in a pre-martensitic state can be described using the short-range order of atomic displacements in terms of the type of the future martensitic phase mainly by means of the correlated and shear displacements along the $\{101\}<101>_{BCC}$ system followed by the formation of nanolocalized tweed substructures.

This work has been performed within the framework of the terms of reference "Structure" No. AAAA-A18-118020190116-6, and was partially supported from the RFBR project No. 18-32-00529 mol_a.

REFERENCES

1. V. N. Khachin, V. G. Pushin, and V. V. Kondratiev, Titanium Nickelide. Structure and Properties [in Russian], Nauka, Moscow (1992).
2. V. G. Pushin, V. V. Kondratiev, and V. N. Khachin, Pre-transitional Phenomena and Martensitic Transformations [in Russian], UrD RAS (1998).
3. A. I. Potekaev, A. A. Klopotov, E. V. Kozlov, and V. V. Kulagina, Low-Stability Pre-transitional Structures in Titanium Nickelide [in Russian], NTL Publ., Tomsk (2004).
4. P. L. Potapov, Scripta Metallurg. et Material., **31**, No. 9, 1243–1248 (1994).
5. P. L. Potapov, N. A. Polyakova, V. A. Udovenko, *et al*., Z. Metallk., **87**, Iss. 1, 33–39 (1996).
6. D. Schryvers, J. Phys. IV France, **7**, No. C5, 109–118 (1997).
7. E. S. Belosludtseva, N. N. Kuranova, N. I. Kourov, *et al*., Tech. Phys., **60**, Iss. 9, 1330–1334 (2015).
8. Z. Y. Wei, E. K. Liu, J. H. Chen, *et al*., Appl. Phys. Lett., **107**, Iss. 2, 022406-1–022406-5 (2015).
9. V. G. Pushin, N. N. Kuranova, E. V. Marchenkova, *et al*., Tech. Phys., **58**, Iss. 6, 878–887 (2013).
10. Yu. V. Khlebnikova, L. Yu. Egorova, D. P. Rodionov, *et al*., Tech. Phys., **61**, Iss. 6, 887–897 (2016).
11. V. D. Klopotov, A. A. Klopotov, A. I. Potekaev, *et al*., Bull. Tomsk Polytech. Univer., **311**, No. 2, 120–125 (2011).
12. Ni–Mn–Ti Diagram, Springer Materials at: https://materials.springer.com/periodictable#Mn-Ni-Ti.